

# Decoherence and single electron charging in an electronic Mach-Zehnder interferometer

L. V. Litvin,\* H.-P. Tranitz, W. Wegscheider, and C. Strunk

*Institut für Experimentelle und Angewandte Physik, Universität Regensburg, D-93040 Regensburg, Germany*

(Received 7 November 2006; revised manuscript received 24 November 2006; published 25 January 2007)

We investigate the temperature and voltage dependence of the quantum interference in an electronic Mach-Zehnder interferometer using edge channels in the integer quantum-Hall regime. The amplitude of the interference fringes is significantly smaller than expected from theory; nevertheless the functional dependence of the visibility on temperature and bias voltage agrees very well with theoretical predictions. Superimposed on the Aharonov-Bohm (AB) oscillations, a conductance oscillation with a six times smaller period is observed. The latter depends only on gate voltage and not on the AB phase, and may be related to single electron charging.

DOI: [10.1103/PhysRevB.75.033315](https://doi.org/10.1103/PhysRevB.75.033315)

PACS number(s): 73.23.Ad, 73.63.Nm

Electron interferences in mesoscopic conductors manifest themselves in conductance oscillations which are  $h/e$  periodic in the magnetic field  $B$ .<sup>1</sup> In conventional metals the visibility  $\nu_I$  of these Aharonov-Bohm (AB) oscillations typically amounts to  $\nu_I = G_0/G \approx 10^{-3}$ , where  $G$  is the conductance of the sample and  $G_0 = 2e^2/h$  the conductance quantum. The visibility can be enhanced to  $\nu_I \approx 0.1$  by reducing the number of conductance channels, e.g., in nanostructures based on two-dimensional electron systems<sup>2,3</sup> containing only a small number of conductance channels. Recently an electronic analog<sup>4</sup> of the well-known optical Mach-Zehnder interferometer (MZI) was realized, which employs the one-dimensional edge channels in the integer quantum Hall regime.<sup>5</sup> In these devices single channel interference can be realized, while backscattering processes are suppressed. This results in measured visibilities up to  $\nu_I \approx 0.6$ . Such devices open a path for the realization of fundamental two-particle interference experiments in the spirit of Hanbury-Brown and Twiss,<sup>6</sup> as recently proposed.<sup>7</sup>

We have realized MZIs similar to those in Ref. 5. A quantum point contact (QPC) is used to partition an edge channel leaving contact S in two paths. After propagation of the edge channel along the inner and outer edge of a ring-shaped mesa, the two paths are brought to interference at a second QPC, resulting in two output channels D1 and D2 of the interferometer (see Fig. 1). The phase of the two partial waves can be changed both by magnetic field and by an electrostatic gate G. The measured visibility is much smaller than expected from theory<sup>8</sup> and reported in Ref. 5. Despite this quantitative disagreement, the functional dependence of  $\nu_I$  on  $T$  and  $V_{\text{bias}}$  fits very well the simple model of Ref. 8. In addition to the AB oscillations we found another type of conductance oscillations, which have a significantly smaller period in gate voltage when compared to the AB period.

The mesa was prepared through wet etching of a modulation doped GaAs/Ga<sub>x</sub>Al<sub>1-x</sub>As heterostructure containing a two-dimensional electron system (2DES) 90 nm below the surface. At 4 K, the unpatterned 2DES density and mobility were  $n = 2.0 \times 10^{15} \text{ m}^{-2}$  and  $\mu = 206 \text{ m}^2/(\text{V s})$ , respectively. Using standard electron beam lithography techniques, we prepared split gates connected by air bridges, defining QPCs of 500 nm length and 220 nm gap width. The measurements were performed in a dilution refrigerator with two stages of

copper powder filters at bath temperature and at 100 mK. The currents at contacts D1 and D2 were measured using a lock-in technique with an ac excitation voltage (1 kHz) of 10–16  $\mu\text{V}$  applied to contact S. We checked that the measured visibilities remained constant below this level of the voltage. The output of a current preamplifier (DL-1211) was controlled with a spectrum analyzer. The stray peaks originating from 50 Hz harmonics and cryostat vibration were smaller than 1  $\mu\text{V}$ .

To characterize the samples, we first verified that the current through contact D1 goes to zero when the filling factor  $\nu$  approaches 1 or 2 (see Fig. 2). This implies a complete suppression of backscattering between the edge channels at the opposite edges of the mesa (Fig. 2, curve D1). The sum of both detector currents,  $I_{D1} + I_{D2}$  shows quantized current (conductance) levels which allow us to determine the value of  $\nu$ . From the position of the minima in current D1 (marked by vertical arrows in Fig. 2) at magnetic fields  $B_\nu = \frac{nh}{\nu e}$  for  $\nu = 3, 4, 6$  we determine an electron density  $n = 1.7 \times 10^{15} \text{ m}^{-2}$  which is 15% smaller than that of the unpatterned 2DES because of the depletion near the mesa edges. If we apply a negative voltage at one of the QPCs at  $\nu \approx 2$ , the inner edge channel starts to split into two branches flowing into D1 and D2. When the QPC is pinched off the current will be completely redirected from D2 into D1. Then, the conductance  $G_{S,D1}$  will be close to  $2e^2/h$  (inset to Fig. 2). In our experiment the conductance  $G_{S,D1}$  at the plateau reaches about 95%

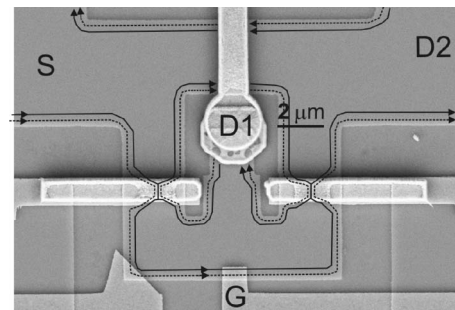


FIG. 1. Scanning electron microscopy image of a Mach-Zehnder interferometer with the scheme of edge states for filling factor 2. The inner edge channel (full line) is split into two branches using QPCs.

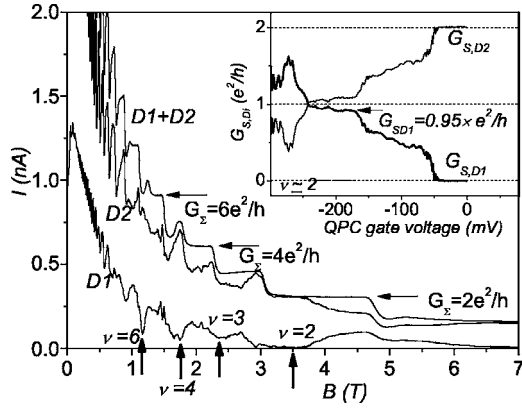


FIG. 2. The currents collected by D1, D2 and their sum as a function of magnetic field at  $V_{\text{bias}}=4 \mu\text{V}$  and  $T=25 \text{ mK}$ , when both QPCs are open. The thick vertical arrows show magnetic fields corresponding to the indicated filling factors; the horizontal arrows label conductance level. Inset: two point conductance between contacts S, D1 and S, D2 as a function of gate voltage at one of the QPCs for  $B=3.26 \text{ T}$ ; the second QPC is open.

of ( $e^2/h$ ). This implies a high transmission of the miniature ohmic contact D1, reflecting only 5% of the incident current back into the edge channel.

To observe interference both QPCs were tuned to transmission 1/2 for the inner edge channel (full line in Fig. 1). The currents at D1 and D2 as a function of gate voltage  $V_G$  are shown in Figs. 3(a) and 3(b), respectively. Current conservation requires that the oscillations detected in D1 and D2 should go in antiphase and sum up to a constant value [Fig. 3(c)]. Two periods of oscillation are seen in these traces. The

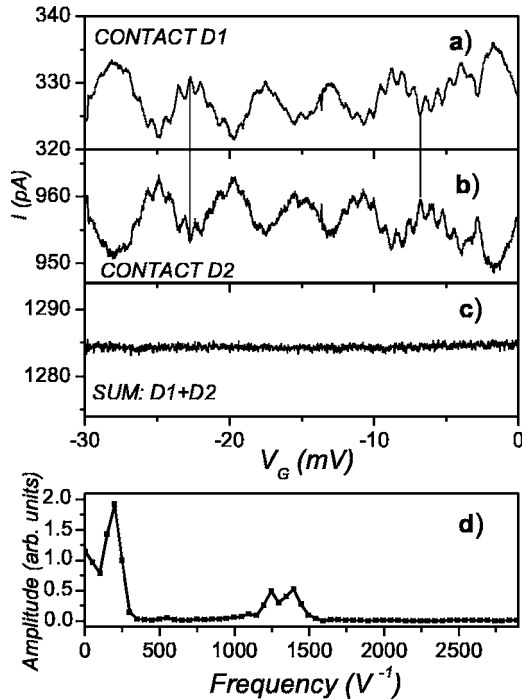


FIG. 3. The currents collected by D1 (a), D2 (b), and their sum (c) as a function of gate  $G$  voltage at  $T=25 \text{ mK}$ ,  $B=3.27 \text{ T}$  ( $\nu=2.14$ ). (d) Typical Fourier spectrum of oscillations.

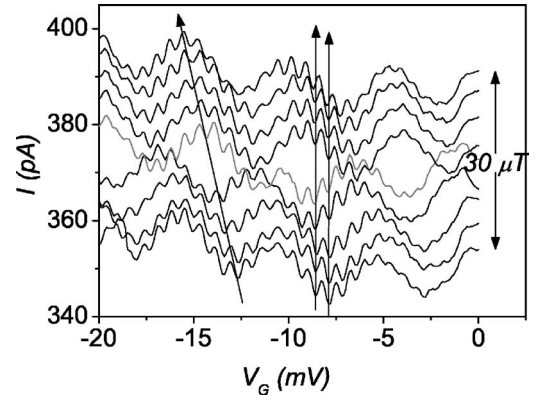


FIG. 4. The time evolution of oscillation at  $T=25 \text{ mK}$ ,  $B=3.27 \text{ T}$  ( $\nu=2.14$ ) indicated by the gradual decay of magnetic field in persistent mode. Successive traces are recorded with 10 min time delay (traces are vertically shifted for clarity by 5 pA). The arrows indicate the progressing recording time and the time shift of the oscillations. The gray curve in the middle displays a phase lapse by  $\pi$  at  $V_G=-11 \text{ mV}$  and separates two trains with linear phase evolution.

amplitude of the small period oscillations is not constant and shows a beatinglike pattern. Fourier analysis reveals two periods of 0.71 and 0.80 mV for the small period oscillations and a period of 5.1 mV for the large period oscillations [Fig. 3(d)]. Since the AB-period  $h/e$  estimated from the area enclosed by the edge channels amounts to  $78 \mu\text{T}$ , a direct measurement of the magnetic field dependence of the interference pattern requires control of the magnetic field at a level of  $10^{-6}$ . Since this is difficult to achieve, we have exploited the gradual decay of the magnetic field in a persistent mode at a rate of about  $20 \mu\text{T/h}$ . In this way the time delay between successive traces can be translated into changes of  $B$ . In Fig. 4 we show a sequence of gate sweeps recorded with time delays of 10 min. The large period oscillations shift linearly with time delay to the left, indicating that these oscillations are of the expected Aharonov-Bohm type. Besides the regular oscillations we observed an occasional switching of the phase of the large period oscillation by  $\approx \pi$  (see, e.g., dashed line in Fig. 4). We attribute these events to slow random transitions of charged impurities between two metastable states. The maximum visibility for the observed AB oscillations was 1.5%. In contrast to these, the small period oscillations do not shift with time and thus do not depend on magnetic field (Fig. 4). This fact points towards an electrostatic origin of this effect.

We now discuss the decay of the oscillation amplitude with temperature and bias voltage. The temperature dependence of the amplitude for both types of oscillations is displayed in Fig. 5. The amplitude of the AB oscillation was averaged first over a few oscillations in a single trace and then over four sweeps taken at each temperature. The amplitude of the small period oscillations was calculated by integrating the Fourier spectrum within a region including both high frequency peaks, i.e., from 1200 to 1450  $\text{V}^{-1}$ . From Fig. 5 we can infer a characteristic energy  $E_C \approx 9 \mu\text{eV}$  (corresponding to  $T_C=100 \text{ mK}$ ) related to the small period oscillation. The peak at higher frequency (1400  $\text{V}^{-1}$ ) decays more

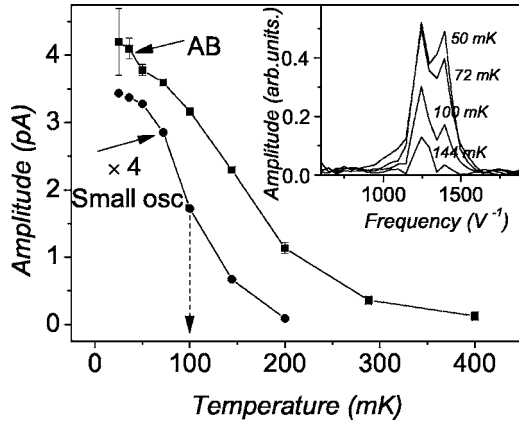


FIG. 5. Measured amplitude of Aharonov-Bohm (squares) and small period oscillations (circles) as a function of temperature. Inset: Evolution of the spectrum of the small oscillations with temperature.

rapid than the peak at  $1250 \text{ V}^{-1}$  both with increasing temperature (inset in Fig. 5) and bias voltage.

According to Ref. 8 the visibility of the AB oscillations  $\nu_I = (I_{\max} - I_{\min}) / (I_{\max} + I_{\min})$  decays with the temperature or voltage as

$$\nu_I = \frac{1}{2} \frac{4\pi k_B T}{eV_{\text{bias}}} \left[ \sinh\left(\frac{k_B T \pi}{E_b}\right) \right]^{-1} \left| \sin\left(\frac{eV_{\text{bias}}}{2E_b}\right) \right|. \quad (1)$$

The prefactor  $1/2$  corresponds to QPC transmission probabilities  $\mathcal{T}_A = \mathcal{T}_B = 1/2$ . The  $T$ - and  $V_{\text{bias}}$ -dependence scales with another characteristic energy  $E_b$ .  $E_b$  determines the phase an electron acquires traversing the asymmetric interferometer with a difference  $\Delta L$  in path length between the two interferometer arms. An electron at energy  $E$  above the Fermi energy  $E_F$  collects a phase difference  $\Delta\phi(E) = \Delta\phi(E_F) + E/E_b$ , where  $E_b \approx \hbar v_D / (\Delta L)$  and  $v_D$  being the drift velocity. The energy dependence of this phase difference smears the interference pattern when the interfering electrons are spread over energy ranges  $k_B T$  and  $eV_{\text{bias}}$ . This is in complete analogy to the interference of a polychromatic light beam in optics. Equation (1) well reproduces the shape of the measured curves (Fig. 6) but not the absolute value of the visibility. The latter is 80 times smaller in our experiment.

The values of  $E_b \approx 18 \mu\text{eV}$  extracted from the fit of the  $T$ - and  $V_{\text{bias}}$ -dependence of Eq. (1) to the data coincide within 3% accuracy. The theory assumes a dc voltage bias, while we used an ac bias in the experiment. Averaging over the ac bias window results in the solid line in Fig. 6(b), which is again in complete agreement with the data.

Next we connect the energy scales  $E_C$  and  $E_b$  with the geometric parameters of our device. From the location of the inner edge channel we can deduce the path difference  $\Delta L$  between the two interferometer arms, which determines  $E_b$ . Taking into account the depletion region at the mesa edge we estimate the distance between the mesa edge and the location of the inner edge channel. Our estimate is based on the electron density extracted from the positions of current minima at the integer filling factor in D1 (see Fig. 2) for the MZIs

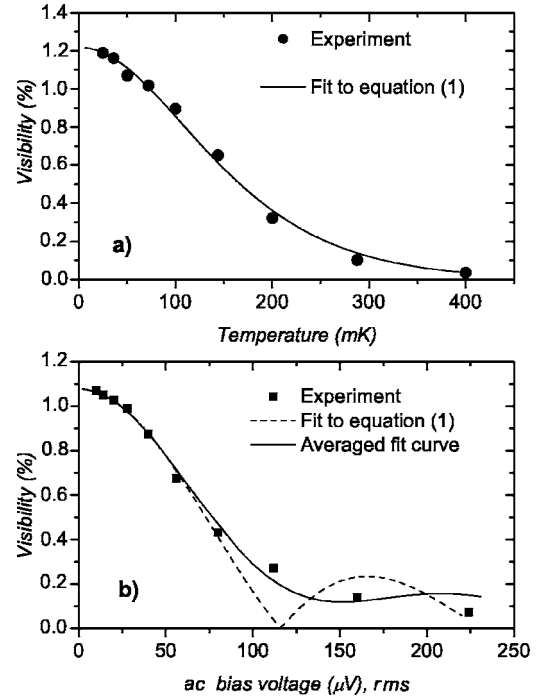


FIG. 6. Visibility decay as a function of (a) temperature ( $V_{\text{bias}} = 16 \mu\text{V}$ , rms) and (b) voltage ( $T = 25 \text{ mK}$ ). In (b) fitting was carried out in the  $V_{\text{bias}}$ -range  $0-80 \mu\text{V}$ .

with the arm width of  $2.5$  and  $1.7 \mu\text{m}$ . Using the edge reconstruction model,<sup>10</sup> we find a depletion length of  $2l = 180 \text{ nm}$ , a distance between the mesa edge and the center of the incompressible strip  $x_1 = 150 \text{ nm}$  (for  $\nu = 2$ ), and the width of incompressible strip  $a_1 = 45 \text{ nm}$ . This results in a distance  $l + x_1 + a_1/2 = 260 \text{ nm}$  between the mesa edge and the inner edge strip for our interferometer, implying that the length of the two interferometer arms differs by about  $\Delta L = 2.0 \mu\text{m}$ . The known  $E_b$  and  $\Delta L$  yield the drift velocity of  $5 \times 10^4 \text{ m/s}$  which agrees well with other estimates<sup>11</sup> for the edge state regime.

The question remains, why the measured visibility of the AB oscillations for our interferometer is so small. It can be seen from Fig. 6 that  $\nu_I$  remains temperature dependent down to  $50 \text{ mK}$ . Although a reduction of the ac bias voltage did not improve the visibility, we cannot exclude other sources of dephasing. On the other hand an intrinsic source of dephasing may result from the internal degrees of freedom of the QPC,<sup>12</sup> which sensitively depend of the shape of the QPC potential. In our case the QPCs consist of rather long ( $500 \text{ nm}$ ) and narrow ( $200 \text{ nm}$ ) channels, which are quite different from an ideal saddle point potential.

In earlier experiments, a very high interference visibility of 60% was reported.<sup>5,9</sup> This value rapidly dropped down to 1% when increasing the temperature from  $20$  to  $100 \text{ mK}$ , indicating a relevant energy scale  $E_b$  even smaller than in our experiment. A satisfactory agreement between these experiments with simple theoretical models<sup>8</sup> is still lacking, since the data of Ref. 9 indicate a surprising independence of the visibility on the asymmetry between the interferometer arms.

We now return to the small oscillations and their characteristic energy  $E_C$ . The striking periodicity of these oscilla-

tions may suggest Coulomb blockade as their possible origin. This requires a charging object with a capacitive coupling to the gate which is stronger than that of the inner edge channel. The latter is responsible for the AB interference. The outer edge channel is ballistically transmitted and should not show charging. Since the side gate is expected to shift both edge channels without qualitative changes in their structure, we see no obvious candidate for such a charging object, unless a relatively large puddle of electrons is formed underneath the gate. We do not have independent evidence that this may happen. On the other hand, the splitting of the observed frequency may suggest that this oscillation is related to the presence of two edge channels in the structure.

In conclusion, we investigated single channel interference

in electronic Mach-Zehnder interferometers and found a strong and unexpected decoherence. Although the absolute value of the measured visibility is a factor of 80 smaller than expected, the functional form of its suppression by finite temperature, bias voltage, and asymmetry of two interfering paths agrees well with a simple model. In addition, we found a second type of oscillation which appears to be of electrostatic origin. This effect requires further investigation.

We thank M. Heiblum, J. Weis, F. Marquardt, S. Ludwig, and J. Kotthaus for stimulating discussions. This work was supported by the Deutsche Forschungsgemeinschaft in the framework of Project No. SFB631 "Solid state quantum information processing."

---

\*On leave from Institute of Semiconductor Physics, 630090, Novosibirsk, Russia.

<sup>1</sup>For a review see, e.g., S. Washburn and R. A. Webb, *Rep. Prog. Phys.* **55**, 1311 (1992).

<sup>2</sup>M. Casse, Z. D. Kvon, G. M. Gusev, E. B. Olshanetskii, L. V. Litvin, A. V. Plotnikov, D. K. Maude, and J. C. Portal, *Phys. Rev. B* **62**, 2624 (2000).

<sup>3</sup>A. E. Hansen, A. Kristensen, S. Pedersen, C. B. Sorensen, and P. E. Lindelof, *Phys. Rev. B* **64**, 045327 (2001).

<sup>4</sup>G. Seelig and M. Büttiker, *Phys. Rev. B* **64**, 245313 (2001).

<sup>5</sup>Y. Ji, Y. Chung, D. Spinzak, M. Heiblum, D. Mahalu, and H. Shtrikman, *Nature (London)* **422**, 415 (2003).

<sup>6</sup>R. Hanbury Brown and R. Q. Twiss, *Nature (London)* **178**, 1046 (1956).

<sup>7</sup>P. Samuelsson, E. V. Sukhorukov, and M. Büttiker, *Phys. Rev. Lett.* **92**, 026805 (2004).

<sup>8</sup>V. S.-W. Chung, P. Samuelsson, and M. Büttiker, *Phys. Rev. B* **72**, 125320 (2005).

<sup>9</sup>I. Neder, M. Heiblum, Y. Levinson, D. Mahalu, and V. Umansky, *cond-mat/0508024*; *Phys. Rev. Lett.* **96**, 016804 (2006).

<sup>10</sup>D. B. Chklovskii, B. I. Shklovskii, and L. I. Glazman, *Phys. Rev. B* **46**, 4026 (1992).

<sup>11</sup>S. Komiyama, H. Hirai, S. Sasa, and S. Hiyamizu, *Phys. Rev. B* **40**, 12566 (1989).

<sup>12</sup>See, e.g., S. M. Cronenwett, H. J. Lynch, D. Goldhaber-Gordon, L. P. Kouwenhoven, C. M. Marcus, K. Hirose, N. S. Wingreen, and V. Umansky, *Phys. Rev. Lett.* **88**, 226805 (2002), and references therein.